

Synthesis, characterization and photovoltaic properties of poly(cyclopentadithiophene-*alt*-isoindigo)<sup>†</sup>Cite this: *Polym. Chem.*, 2013, **4**, 5351Chun-Chih Ho,<sup>ab</sup> Sheng-Yung Chang,<sup>c</sup> Tzu-Chia Huang,<sup>d</sup> Chien-Ann Chen,<sup>d</sup> Hsueh-Chung Liao,<sup>a</sup> Yang-Fang Chen<sup>c</sup> and Wei-Fang Su<sup>\*bd</sup>

Isoindigo based conducting polymers have attracted extensive interest for polymer solar cell application since isoindigo is a green material and renewable from plants. We have synthesized four soluble low band gap isoindigo based polymers (PCI) with cyclopentadithiophene (CPDT) as the donor unit and isoindigo (I) as the acceptor unit, decorated with two kinds of alkyl side chains, octyl (8) and 2-ethylhexyl (e), via the Stille cross-coupling reaction denoted as PC8I8, PC8Ie, PCeI8 and PCeIe. By changing the side chain of copolymers from linear (PC8I8) to branched (PCeIe), the  $\lambda_{\text{max}}$  of absorption is blue shifted from 1.37 to 1.48 eV and the HOMO level is lowered from  $-5.24$  to  $-5.45$  eV. The changes are due to the twist coplanarity of the polymer backbone. The density functional theory calculation revealed that the dihedral angle of copolymers has been increased from  $14^\circ$  to  $20^\circ$ . The properties of PC8Ie and PCeI8 lie between those of PC8I8 and PCeIe. The type of the side chain plays a major role in determining the photovoltaic performance of copolymers. The branched side chain improves the solubility of the polymer and increases the effective phase separation between the copolymer and PCBM. This results in favorable nanomorphology of the active layer. Thus, PCeIe with branched side chains on both donor and acceptor units exhibits the best photovoltaic properties with a  $V_{\text{oc}}$  of 0.80 eV,  $J_{\text{sc}}$  of  $11.6 \text{ mA cm}^{-2}$  and fill factor of 43.0% and power conversion efficiency of 4.0%. The power conversion efficiency of this type of polymer could be further improved by optimizing the fabrication conditions and interlayer modification. This study offers a useful guideline for the molecular design of high efficiency isoindigo-based polymer solar cells.

Received 23rd January 2013  
Accepted 12th April 2013

DOI: 10.1039/c3py00119a

[www.rsc.org/polymers](http://www.rsc.org/polymers)

## Introduction

Polymer solar cells (PSCs) as an alternative to inorganic photovoltaic devices have become the focus of intense research due to their lightweight, flexibility and ease of large-scale fabrication.<sup>1–4</sup> A typical PSC of the active layer is usually based on the bulk heterojunction (BHJ) concept and is fabricated from blending of the electron donor (conducting polymers) and electron acceptor (fullerene derivatives).<sup>5</sup> To achieve a high efficiency BHJ solar cell, several factors in molecular structures (*e.g.*, conjugated backbone and side chains) must be rationally designed for the polymer.<sup>6</sup> The donor–acceptor (D–A) strategy is

widely applied to design the backbone of the conjugated polymer. By combination of the electron-donating moiety and electron-withdrawing moiety, the energy level of the resulting alternating conjugated copolymer can be fine-tuned through intramolecular charge transfer (ICT) and lead to a narrow band gap (1.2–1.8 eV) and thereby can absorb more light in the visible and infrared region. Although vast D–A low band gap polymers were developed,<sup>7</sup> it is still a challenge to develop an ideal and sustainable low band gap polymer with appropriate choice of donor and acceptor units.

Isoindigo is a kind of sustainable chemical which is available from natural plants,<sup>8,9</sup> so we call the copolymer derived from isoindigo a green polymer. The isoindigo has strong electron-withdrawing ability due to the diimide functional group. Many isoindigo based D–A conjugated polymers have been reported.<sup>10–17</sup> The results indicate that the isoindigo based D–A conjugated polymers exhibit promising broad absorption, well matched energy level with PCBM acceptors and high charge mobility,<sup>18</sup> showing that isoindigo can be a promising acceptor unit for constructing ideal D–A conjugated polymers. The solubilizing side chains attached on the backbone of the isoindigo copolymer are necessary for the ease of solar cell fabrication. However, the systematic study of solubilizing side

<sup>a</sup>Department of Materials Science and Engineering, National Taiwan University, Taipei, 10617, Taiwan<sup>b</sup>Graduate Institute of Photonics and Optoelectronics, National Taiwan University, Taipei, 10617, Taiwan. E-mail: suwf@ntu.edu.tw; Fax: +886 2 33664078; Tel: +886 2 33664078<sup>c</sup>Graduate Institute of Applied Physics, National Taiwan University, Taipei, 10617, Taiwan<sup>d</sup>Institute of Polymer Science and Engineering, National Taiwan University, Taipei, 10617, Taiwan<sup>†</sup> Electronic supplementary information (ESI) available. See DOI: 10.1039/c3py00119a

chain effects on the solar cell performance of the isoindigo-based D–A conjugated polymer cell is lacking. It is imperative to understand their role in the active layer of the solar cell. In addition to enhancing the solubility of the copolymer, the side chain affects the band gap of the copolymer, the miscibility with PCBM, optoelectronic properties, nanomorphology and photovoltaic performance of the resulting PSC.<sup>19–23</sup> Therefore, establishing comprehensive knowledge of the side chain effects on the rational design polymer for high efficiency isoindigo based polymer solar cells is necessary.

In this work, we used cyclopentadithiophene (CPDT) as a donor unit and isoindigo as an acceptor unit to design and synthesize a series of low band gap copolymers containing different structures of alkyl side chains either on a cyclopentadithiophene unit or isoindigo unit. These specific donors and acceptors were chosen because these monomers are able to satisfy the concept of a strong acceptor and a weak donor.<sup>24</sup> The resulting polymers are expected to be ideal polymers which can be blended with PCBM for potential high performance solar cells.<sup>25</sup> Furthermore, these monomers can also be synthesized in large quantity by using facile methods reported by B. Y. Lee and J. H. Park for the CPDT monomer<sup>26</sup> and J. R. Reynolds *et al.* for the isoindigo monomer.<sup>9</sup> The resulting polymers exhibit broad absorption as predicted and have a band gap around 1.5 eV. The steric hindrance effect caused by the type of side chain has a significant influence on the ICT state and optical band gap. These behaviors are also supported by the theoretical calculation. From the electrochemical property results, the HOMO energy level of the copolymer can be adjusted by tuning the coplanarity of the copolymers, whereas the effect on the LUMO energy level is to a lesser extent. Finally, various blend ratios of the copolymer with PCBM related to the morphology and cell performance were investigated. It is interesting to find that the type of side chain has a larger effect on the acceptor unit than the donor for the optimized blend ratio. The detailed results and discussion are presented below.

## Experimental

### Materials

Isopropylmagnesium chloride (2.0 M solution in THF) (i-PrMgCl), lithium chloride (99%) (LiCl), diethyl oxalate (99%), aluminum chloride (98.5%) (AlCl<sub>3</sub>), potassium iodide (99%) (KI), 1-bromooctane (99%), 2-ethylhexyl bromide (95%), trimethyltin chloride (1.0 M solution in THF) and tris(dibenzylideneacetone) dipalladium(0) (97%) (Pd<sub>2</sub>(dba)<sub>3</sub>) were purchased from Acros. Tri(*o*-tolyl)phosphine (97%) (P(*o*-tyl)<sub>3</sub>) and diethylammonium diethyldithiocarbamate (97%) were purchased from Aldrich. 3-Bromothiophene (97%) and 6-bromoisatin (95%) were purchased from Matrix Scientific. 6-Bromooxindole (98%) and *n*-butyl lithium (2.5 M solution in hexane) (*n*-BuLi) were purchased from Seedchem and Chemetall, respectively. All purchased chemicals were used without further purification. Tetrahydrofuran (THF) for reaction was dried with Na/benzophenone before being used.

### Synthesis of ethyl 2-oxo-2-(thiophen-3-yl)acetate (1)

2 M i-PrMgCl in THF (109.97 mL, 0.219 mol) was added to the solution of LiCl (16.95 g, 0.399 mol) in 250 mL anhydrous THF. 3-Bromothiophene (18.74 mL, 0.199 mol) was subsequently added to the mixture and stirred for 2 hours at room temperature. The mixture was then added dropwise to the solution of diethyl oxalate (68 g, 0.470 mol) in 200 mL anhydrous THF at –78 °C and stirred at –78 °C for another 2 hours. The resulting white suspension was warmed to –20 °C, hydrolyzed with 5 M HCl (45 mL), poured into ice, and extracted with diethyl ether. Evaporation of the solvent afforded a yellow liquid which was further fractionated under vacuum to give a yellow liquid (96 °C at 0.3 torr) and yield 31.47 g (85%). <sup>1</sup>H NMR (400 MHz, CDCl<sub>3</sub>) δ (ppm) = 8.54 (s, 1H), 7.68 (d, 1H), 7.35 (dd, 1H), 4.42 (dd, 2H), 1.42 (t, 3H).

### Synthesis of ethyl 2-hydroxy-2,2-di(thiophen-3-yl)acetate (2)

2 M i-PrMgCl in THF (100 mL, 0.205 mol) was added to the solution of LiCl (14 g, 0.273 mol) in 250 mL anhydrous THF. 3-Bromothiophene (17.39 mL, 0.171 mol) was subsequently added to the mixture and stirred for 2 hours at room temperature. The mixture was then added dropwise to the THF solution of **1** (31.47 g, 0.171 mol in 200 mL anhydrous THF) at –78 °C and stirred at –78 °C for another 1 hour. The resulting mixture was warmed to 9 °C, hydrolyzed with 5 M HCl (45 mL), poured into water, and extracted with diethyl ether. Evaporation of the solvent afforded the crude product of the yellow liquid (49.18 g), and the <sup>1</sup>H NMR spectrum indicated that the purity (90%) of the crude product was satisfactory to proceed to next step without further purification. <sup>1</sup>H NMR (400 MHz, CDCl<sub>3</sub>) δ (ppm) = 7.34 (m, 2H), 7.28 (m, 2H), 7.14 (d, 2H), 4.32 (m, 2H), 1.05 (t, 3H).

### Synthesis of 2-hydroxy-2,2-di(thiophen-3-yl)acetic acid (3)

The crude product of compound **2** (29.72 g) was dissolved in 10% KOH/methanol solution (KOH, 12 g, 0.212 mol) and stirred for 18 hours at room temperature. The mixture was subsequently poured in water (150 mL) and extracted with diethyl ether (150 mL) two times. Toluene (200 mL) was added to the collected water phase, and H<sub>2</sub>SO<sub>4</sub> (23 g, 0.230 mol) diluted with water (70 mL) was added dropwise while stirred vigorously. The organic phase was collected and the solvent was removed by a rotary evaporator to give a white solid of the crude product. The crude product was further purified by recrystallization with toluene–hexane (1 : 3). (14.09 g, 49%) <sup>1</sup>H NMR (400 MHz, CDCl<sub>3</sub>) δ (ppm) = 7.39 (dd, 2H), 7.31 (dd, 2H), 7.17 (dd, 2H), OH signal is missing due to broadening.

### Synthesis of 4*H*-cyclopenta[1,2-*b*:5,4-*b'*]dithiophene-4-carboxylic acid (4)

To a solution of **3** (14.09 g) in anhydrous toluene, AlCl<sub>3</sub> (23.53 g, 0.179 mol) was added at 4 °C rapidly. The solution was refluxed for 1 hour. Hydrolysis was followed by extraction with saturated Na<sub>2</sub>CO<sub>3</sub> aqueous solution and acidification on the collected water phase. Then the precipitate was filtered to give a light

brown solid (3.55 g, 38%).  $^1\text{H NMR}$  (400 MHz,  $\text{CDCl}_3$ )  $\delta$  (ppm) = 7.20 (dd, 4H), 4.63 (s, 1H).

#### Synthesis of 4,4-bis(2-ethylhexyl)-4*H*-cyclopenta[1,2-*b*:5,4-*b'*]-dithiophene (5a)

Compound 4 (1 g, 4.5 mmol) was dissolved in 20 mL DMSO, and KOH (0.757 g, 13.5 mmol) was added. The mixture was evacuated and then stirred overnight under a closed vacuum system. After overnight stirring, the system was briefly evacuated each hour seven times. Subsequently, 2-ethylhexyl bromide (1.74 g, 9 mmol) and KI (25 mg, 0.15 mmol) were added to the mixture and stirred overnight at room temperature. Water was added to the solution and extracted with hexane. Further purification by column chromatography (silica gel/hexane) gave yellow liquid (1.0 g, 55%).  $^1\text{H NMR}$  (400 MHz,  $\text{CDCl}_3$ )  $\delta$  (ppm) = 7.11 (d, 2H), 6.93 (m, 2H), 1.92–1.81 (m, 4H), 1.40–1.07 (m, 20H), 1.07–0.92 (m, 4H), 0.88 (t, 6H).

#### Synthesis of 4,4-dioctyl-4*H*-cyclopenta[1,2-*b*:5,4-*b'*]-dithiophene (5b)

The procedure is the same as that used for synthesizing compound 5a. With 1-bromooctane (1.74 g, 9 mmol), yielding a yellow liquid (1.05 g, 58%).  $^1\text{H NMR}$  (400 MHz,  $\text{CDCl}_3$ )  $\delta$  (ppm) = 7.14 (d, 2H), 6.93 (d, 2H), 1.81 (t, 4H), 1.35–1.00 (m, 24H), 1.00–0.89 (m, 4H), 0.84 (t, 6H).

#### Synthesis of (4,4-bis(2-ethylhexyl)-4*H*-cyclopenta[1,2-*b*:5,4-*b'*]-dithiophene-2,6-diyl)bis(trimethylstannane) (6a)

Compound 5a (0.4049 g, 1 mmol) was dissolved in dry THF (40 mL), 2.5 M *n*-BuLi in hexane (1.206 mL, 3 mmol) was added at  $-78^\circ\text{C}$ , and stirred for 1 hour at  $-78^\circ\text{C}$ . Subsequently, the mixture was allowed to warm to room temperature and stirred for another 1 hour. After stirring, 1 M trimethyltin chloride in THF (2.11 mL, 2.11 mmol) was added at  $-78^\circ\text{C}$ , and stirred overnight at room temperature. The resulting solution was extracted with hexane, purified by column chromatography (C18-functionized silica gel/hexane–methanol = 1 : 4). A yellow liquid was obtained (0.72 g, 98.6%). The full NMR spectrum of this synthesized compound is shown in Fig. S1.† The spectrum is quite clean without any impurity peaks which indicates that the product has a purity of >95%.  $^1\text{H NMR}$  (400 MHz,  $\text{CDCl}_3$ )  $\delta$  (ppm) = 6.93 (m, 2H), 1.95–1.76 (m, 4H), 1.35–1.2 (m, 2H), 1.10–0.82 (m, 16H), 0.74 (m, 6H), 0.58 (t, 6H), 0.35 (t, 18H).

#### Synthesis of (4,4-dioctyl-4*H*-cyclopenta[1,2-*b*:5,4-*b'*]-dithiophene-2,6-diyl)bis(trimethylstannane) (6b)

The procedure is the same as that used for synthesizing compound 6a. With compound 5b (0.30 g, 1.35 mmol), a yellow liquid was obtained (0.48 g, 89%). The full NMR spectrum of this synthesized compound is shown in Fig. S2.† The spectrum is quite clean without any impurity peaks which indicates that the product has a purity of >95%.  $^1\text{H NMR}$  (400 MHz,  $\text{CDCl}_3$ )  $\delta$  = 6.94 (m, 2H), 1.78 (m, 4H), 1.21 (m, 20H), 0.85 (m, 10H), 0.38 (t, 18H).

#### Synthesis of 6,6'-dibromoisindigo (7)

6-Bromooxindole (10 g, 0.047 mol) and 6-bromoisatin (10.66 g, 0.047 mol) were added to acetic acid (300 mL), and then conc. HCl solution (2 mL), refluxed for 24 hours. The mixture was cooled, filtered and washed with water, ethanol and ethyl acetate to give a dark brown solid (18.6 g, 93%).  $^1\text{H NMR}$  (400 MHz,  $d_6$ -DMSO)  $\delta$  (ppm) = 11.08 (s, 2H), 8.98 (d, 2H), 7.17 (dd, 2H), 6.98 (s, 2H).

#### Synthesis of *N,N'*-bis(2-ethylhexyl)-6,6'-dibromoisindigo (8a)

Compound 7 (15 g, 0.036 mol) and  $\text{K}_2\text{CO}_3$  (29.6 g, 0.178 mol) were added to dry DMF (700 mL). 2-Ethylhexyl bromide (14.01 mL, 0.079 mol) was added to the mixture under nitrogen and stirred at  $100^\circ\text{C}$  for 15 hours. The mixture is cooled to room temperature and extracted with  $\text{CH}_2\text{Cl}_2$ . Further purification by column chromatography (silica gel/ $\text{CH}_2\text{Cl}_2$ –hexane = 1 : 3) gave dark red solids (19.57 g, 85%). The full NMR spectrum of this synthesized compound is shown in Fig. S3.† The spectrum is quite clean without any impurity peaks which indicates that the product has a purity of >95%.  $^1\text{H NMR}$  (400 MHz,  $\text{CDCl}_3$ )  $\delta$  (ppm) = 9.00 (d, 2H), 7.13 (dd, 2H), 6.81 (d, 2H), 3.60–3.48 (m, 4H), 1.90–1.72 (m, 2H), 1.43–1.20 (m, 16H), 0.95–0.82 (m, 12H).

#### Synthesis of *N,N'*-dioctyl-6,6'-dibromoisindigo (8b)

8b was synthesized according to the same procedure as that of 8a using octyl bromide instead of 2-ethylhexyl bromide. The full NMR spectrum of this synthesized compound is shown in Fig. S4.† The spectrum is quite clean without any impurity peaks which indicates that the product has a purity of >95%.  $^1\text{H NMR}$  (400 MHz,  $\text{CDCl}_3$ )  $\delta$  (ppm) = 9.07 (d, 2H), 7.16 (dd, 2H), 6.92 (d, 2H), 3.72 (t, 4H), 1.86–1.59 (m, 4H), 1.32 (dd, 20H), 0.87 (t, 6H).

#### Synthesis of PC8I8

Compound 6a (0.2 g, 0.497 mmol), 8b (0.17 g, 0.264 mmol),  $\text{Pd}_2(\text{dba})_3$  (5 mg) and  $\text{P}(o\text{-tyl})_3$  (13 mg) were added to the microwave reactor tube and sealed in the glove box. Dry *o*-xylene (5 mL) was subsequently added to the tube. The tube was subjected to the microwave reactor and stirred under conditions of  $150^\circ\text{C}$ , 300 W for one hour. After that, diethylammonium diethyldithiocarbamate was added and stirred at  $60^\circ\text{C}$  for 15 minutes. After being cooled to room temperature, the reaction medium was precipitated into methanol and collected *via* filtration. The precipitate was purified *via* Soxhlet extraction with methanol, acetone and hexane to remove catalyst residues and low molecular weight fractions. Then the residue solids were dried *via* vacuum, yielding dark-red solids. The full NMR spectrum of this synthesized copolymer is shown in Fig. S5.† The spectrum is quite clean without any peaks of impurities which indicates that the product has a purity of >95%.  $^1\text{H NMR}$  (400 MHz,  $\text{CDCl}_3$ )  $\delta$  = 9.30–8.60 (br, 2H), 7.52–7.28 (br m, 4H), 6.98–6.30 (br m, 2H), 3.78 (br m, 4H), 2.40–0.35 (br m, 68H).

### Synthesis of PC8Ie

The procedure is the same as that used for PC8I8 but using compounds **8a** (0.35 g, 0.549 mmol) and **6b** (0.40 g, 0.549 mmol), Pd<sub>2</sub>(dba)<sub>3</sub> (10.0 mg, 0.011 mmol) and P(*o*-tyl)<sub>3</sub> (26.7 mg, 0.088 mmol). Dark red solids were obtained (0.2 g). The full NMR spectrum of this synthesized copolymer is shown in Fig. S6.† The spectrum is quite clean without any peaks of impurities which indicates that the product has a purity of >95%. <sup>1</sup>H NMR (400 MHz, CDCl<sub>3</sub>) δ = 9.18 (br m, 2H), 7.52–7.28 (br m, 4H), 6.98–6.30 (br m, 2H), 3.78 (br m, 4H), 2.40–0.35 (br m, 68H).

### Synthesis of PCeI8

The procedure is the same as that used for PC8I8 but using compounds **8b** (0.35 g, 0.549 mmol) and **6b** (0.40 g, 0.549 mmol), Pd<sub>2</sub>(dba)<sub>3</sub> (10.0 mg, 0.011 mmol) and P(*o*-tyl)<sub>3</sub> (26.7 mg, 0.088 mmol). Dark red solids were obtained (0.2 g). The full NMR spectrum of this synthesized copolymer is shown in Fig. S7.† The spectrum is quite clean without any peaks of impurities which indicates that the product has a purity of >95%. <sup>1</sup>H NMR (400 MHz, CDCl<sub>3</sub>) δ = 9.18 (br m, 2H), 7.52–7.28 (br m, 4H), 6.98–6.30 (br m, 2H), 3.78 (br m, 4H), 2.40–0.35 (br m, 68H).

### Synthesis of PCeIe

The procedure is the same as that used for PC8I8 but using compound **8a** (0.35 g, 0.549 mmol) and **6a** (0.40 g, 0.549 mmol), Pd<sub>2</sub>(dba)<sub>3</sub> (10.0 mg, 0.011 mmol) and P(*o*-tyl)<sub>3</sub> (26.7 mg, 0.088 mmol). Dark red solids were obtained (0.2 g). The full NMR spectrum of this synthesized copolymer is shown in Fig. S8.† The spectrum is quite clean without any peaks of impurities which indicates that the product has a purity of >95%. <sup>1</sup>H NMR (400 MHz, CDCl<sub>3</sub>) δ = 9.18 (br m, 2H), 7.52–7.28 (br m, 4H), 6.98–6.30 (br m, 2H), 3.78 (br m, 4H), 2.40–0.35 (br m, 68H).

### Denotation

C8: CPDT with *n*-octyl side chain; Ce: CPDT with 2-ethylhexyl side chain; I8: isoindigo with *n*-octyl side chain; Ie: isoindigo with 2-ethylhexyl side chain.

### Characterization and measurements

<sup>1</sup>H NMR spectra were recorded on a Bruker DPX400 400 MHz spectrometer and CDCl<sub>3</sub> and d<sub>6</sub>-DMSO were used as a solvent. The molecular weight and molecular weight distribution of synthesized polymers were measured using a Viscotek GPCmax and THF used as an eluent at 35 °C and polystyrene as the standard. The optical properties of all synthesized polymers were measured using a Perkin Elmer Lambda 35 UV/VIS spectrometer. The solution state measurement samples were prepared from dissolving polymers in chlorobenzene (CB) with concentration at 10<sup>-5</sup> to 10<sup>-7</sup> wt%. The solid state samples were prepared by spin-coating 10 mg mL<sup>-1</sup> polymer solution in CB onto quartz. The electrochemical property measurements were determined using a CHI 4052 cyclic voltammetry in 0.1 M tetrabutylammonium perchlorate (TBAP) in dry acetonitrile

solution, using ferrocene as the internal standard. The samples were spin-coated onto ITO glass from 10 mg mL<sup>-1</sup> polymer solutions in CB and used as the working electrode. Pt wire is used as the auxiliary electrode and Ag/Ag<sup>+</sup> as the reference electrode. The scan rate was kept at 100 mV s<sup>-1</sup> and the electrolyte solution was bubbled by nitrogen for five minutes before each scan. For surface morphology, the topographic observation of the film sample film was analyzed by AFM (Digital Instruments, Nanoscopes III) using tapping mode. The samples for this measurement were prepared by directly mixing 10 mg isoindigo polymer and 20 mg PCBM in 1 mL CB or 0.970 mL CB + 0.03 mL DIO, then stirred at 70 °C and 350 RPM for 48 hours. The measurement was performed under ambient conditions with a vibration isolation system. Imaging was done by using a commercially available silicon cantilever with a thickness of 5.0 ± 1 μm, a length of 225 ± 10 μm, and a width of 33 ± 7.5 μm, a resonance frequency of 96–175 kHz and a force constant of 5–37 N m<sup>-1</sup>. The scan rate and resolution were set to be 0.5 Hz and 512 × 512 pixel by pixel for every recorded image.

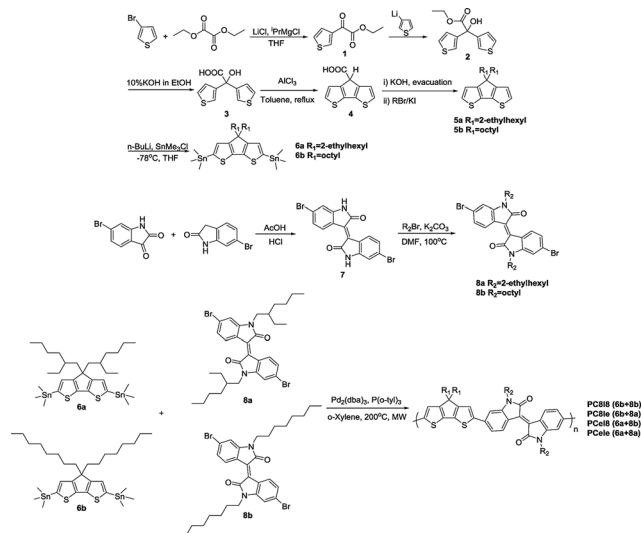
### Devices fabrication and characterization

The polymer-PC61BM solution was prepared by dissolving the polymer and PC61BM in CB with additional 3% of 1,8-diodo-octane (DIO) and then stirred at 70 °C and 350 RPM for 48 hours in a glove box. And an ITO-coated glass substrate was cleaned stepwise by ultrasonic treatment in detergent, methanol, acetone, and isopropyl alcohol. The substrate was further treated by ultraviolet plus oxygen plasma (Harrick Plasma, PDC-001) at a power of 29.6 W for 10 min. Then 40 nm PEDOT:PSS was spin-coated on the cleaned substrate and baked at 120 °C for 20 min. The blend solution was spin-coated on top of the PEDOT:PSS layer at a spin speed of 2200 RPM in air. Finally, the Ca (45 nm) and Al (130 nm) electrodes were deposited on the active layer using a thermal evaporator at <5 × 10<sup>-6</sup> torr. The 12 devices of PC8Ie:PC61BM (1 : 2), PCeI8:PC61BM (1 : 1), and PC8I8:PC61BM (1 : 2), and the 6 devices of PCeIe:PC61BM (1 : 1.5) were fabricated and characterized. The standard deviation of power conversion efficiency (PCE) of the devices for each blend was present.

## Results and discussion

### Synthesis

The synthetic routes of CPDT monomers, isoindigo monomers and polymers are illustrated in Scheme 1. The CPDT monomers were synthesized by adapting the literature methods of B.Y. Lee and J. H. Park<sup>26</sup> and MacDowell *et al.*,<sup>27</sup> the methods are more facile for large-scale synthesis compared to the synthetic route reported by Turner *et al.*,<sup>28</sup> Wynberg *et al.*,<sup>29</sup> Reynolds and Brzezinski,<sup>30</sup> and Marder *et al.*<sup>31</sup> First a Grignard reaction precursor was formed by the reaction of 3-bromothiophene with the turbo Grignard reagent (i-PrMgCl·LiCl complex) and reacted with diethyl oxalate twice to yield compound **2**, followed by subsequent saponification under basic conditions to yield compound **3**. Then compound **3** was cyclized by strong Lewis acid, AlCl<sub>3</sub>, to yield compound **4**. After decarboxylation by KOH



**Scheme 1** Synthetic routes of monomers (CPDT and isoindigo) and polymers (PC8I8, PC8Ie, PCeI8 and PCeIe).

under low vacuum conditions, two different CPDT moieties were obtained by attaching two side chains of 2-ethylhexyl, and *n*-octyl on CPDT, respectively. The isoindigo monomers were prepared according to the literature method<sup>9</sup> and also can be produced on a large scale. The isoindigo usually exhibits poor solubility in common solvents due to the coplanarity, strong  $\pi$ - $\pi$  interactions and hydrogen bonding of the molecule. Therefore, we introduced a linear *n*-octyl side chain and a branched 2-ethylhexyl side chain on both isoindigo and CPDT with different arrangements of side chain types to improve the solubility of copolymers. Four polymers denoted as PC8I8, PC8Ie, PCeI8 and PCeIe were synthesized by microwave-assisted Stille cross-coupling copolymerization of compound **8a** and **8b** with two distannyl compounds **6a** and **6b**, respectively. The first letter "P" in the denotation means polymer, the second letter "C" indicates CPDT, the number "8" is *n*-octyl side chain and the letter "e" is 2-ethylhexyl side chain. The synthesized copolymers were purified *via* Soxhlet extraction with methanol, acetone and hexane to remove catalyst residues and low molecular weight fractions. Note that all materials from monomers to polymers can be produced on a large scale, thus providing the possibility for mass production. The side chains with fixed carbon number were used in this investigation to exclude the diluted effect on the conjugated backbone. These polymers are soluble in common solvents such as tetrahydrofuran (THF), chloroform, chlorobenzene and other chlorinated solvents. The number-average molecular weights ( $M_n$ ), weight-average molecular weights ( $M_w$ ) and polydispersity indices of polymers were determined by gel permeation chromatography (GPC) using polystyrene as a standard and THF as an eluent. GPC data are listed in Table 1. We tried to synthesize the copolymers with a similar number-average molecular weight to minimize the molecular weight effect on their physical properties.

As expected, the branched side chain is more effective to enhance the copolymer solubility than the linear side chain, so

**Table 1** Number-average molecular weight ( $M_n$ ), weight-average molecular weight ( $M_w$ ) and distribution of molecular weights (PDI) of copolymers determined by GPC

Polymer	$M_n$ (Da)	$M_w$ (Da)	PDI
PC8I8	25k	82k	3.34
PC8Ie	20k	50k	2.65
PCeI8	36k	84k	2.29
PCeIe	45k	168k	3.73

the relatively higher molecular weight of PCeIe was obtained as compared to the other three copolymers when the polymerization was carried out in relatively poor solvent of *o*-xylene at a relatively higher solution concentration using a microwave reactor.

### Optical properties

The UV-visible absorption spectroscopy was used to investigate the optical properties of prepared copolymers. Fig. 1 shows the absorption spectra of the copolymers in chlorobenzene (CB) solution and as-cast thin films. The results are summarized in the columns 2, 3, 4 from left of Table 2. All copolymers show two absorption bands both in solution and in film. The high energy absorption band is attributed to the  $\pi$ - $\pi^*$  transition while the low-energy band is related to an intramolecular charge transfer (ICT).

These copolymers show a similar shape of absorption but different  $\lambda_{\max}$  peak positions in solution (Fig. 1a). Compared to PC8I8 having linear side chains on both CPDT and isoindigo units, the coplanarity of PC8Ie, PCeI8 and PCeIe has been perturbed due to the bulky branched 2-ethylhexyl side chains. This led to the reduction of effective ICT and the conjugation length

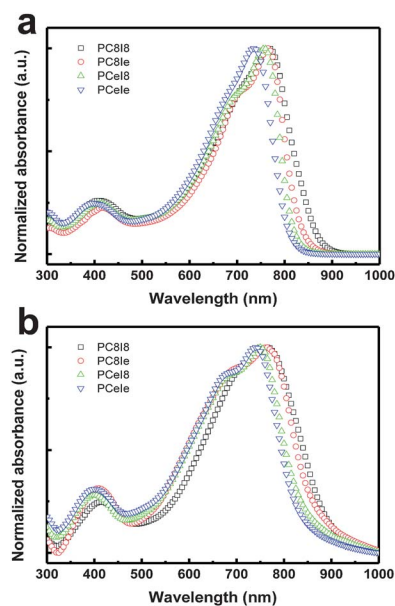


**Fig. 1** UV-Vis absorption spectra of copolymers in (a) chlorobenzene and (b) solid state. Open square: PC8I8; open circle: PC8Ie; open triangle: PCeI8; open inverted triangle: PCeIe.

**Table 2** Summary of optical, electrochemical properties and calculated dihedral angle of copolymers

Polymer	$\lambda_{\max}$ nm (solu.)	$\lambda_{\max}$ nm (solid)	$E_{g,opt}$ (eV)	Dihedral <sup>a</sup> angle (degree)	$E^{ox}$ (V) <sup>b</sup>	$E^{red}$ (V) <sup>b</sup>	HOMO <sup>b</sup> (eV)	LUMO <sup>b</sup> (eV)	$E_g^b$ (eV)
PC8I8	767	765	1.37	14	0.11	-1.24	-5.24	-3.89	1.35
PC8Ie	763	764	1.42	17	0.18	-1.25	-5.31	-3.88	1.43
PCeI8	757	753	1.47	18	0.20	-1.28	-5.33	-3.85	1.48
PCeIe	735	741	1.48	20	0.32	-1.17	-5.45	-3.96	1.49

<sup>a</sup> Theoretical calculation. <sup>b</sup> CV measurement.

and thus their  $\lambda_{\max}$  were blue shifted. The extent of the blue-shift was determined by the coplanarity of the polymer backbone. A larger twist of the polymer backbone occurred when two branched side chains were attached on the same carbon of CPDT (4<sup>th</sup> position) instead of being attached on the two different nitrogen of isoindigo. As a result, PCeI8 and PCeIe with branched side chains attached on CPDT units exhibited larger steric hindrance and showed a larger blue shift than PC8Ie and PC8I8.

In general, a red-shift of absorption should be observed for the polymer in film as compared to that in solution due to the presence of intermolecular  $\pi$ - $\pi$  interactions of the conjugated polymer. However, the  $\lambda_{\max}$  of PC8I8 and PCeI8 films is somewhat blue-shifted. Apparently the longer chain length of the linear *n*-octyl side chain has a larger effect on the spatial arrangement of the copolymers to retard the intermolecular  $\pi$ - $\pi$  interactions as compared to the shorter chain length of branched 2-ethylhexyl side chains, in particular on the isoindigo unit (*i.e.* PCeI8 exhibits the largest blue shift in film). The intermolecular  $\pi$ - $\pi$  interactions are not restricted for PCeIe containing only branched side chains, thus a red shift of 6 nm is observed. We speculate that polymer aggregations are present in all films that resulted in broader absorption and pronounced shoulders of a low-energy absorption band (Fig. 1b). The increase of steric twisting on the conjugated backbone would reduce the effective ICT and increase the optical band gaps of copolymers. Thus, we observe the optical band gap is in the increasing order of 1.37 eV, 1.42 eV, 1.47 eV and 1.48 eV for PC8I8, PC8Ie, PCeI8 and PCeIe respectively as estimated from their onset absorption of the films. These results confirm that the syntheses of low band gap copolymers (<1.5 eV) were successful.

### Theoretical calculations

In order to further investigate the impact of side chain nature on the molecular structure and optoelectronic properties of copolymers, the molecular geometries and the electron density distribution in HOMO and LUMO states of these copolymers were simulated by using the density functional theory (DFT). The DFT simulation was performed using Gaussian 09<sup>32</sup> with the B3LYP functional<sup>33,34</sup> and the 6-31G\* basis set.<sup>35</sup> To reduce the computation time, two repeating units were used as a model for calculations. It should be noted that the free chain ends could have significant influences on the internal dihedral angles of the polymer chain, thus leading to the change of

electronic state and band gap, as reported by previous studies.<sup>36,37</sup> However, these effects could be ignored since the low band gap polymers usually have higher coplanarity. The optimized molecular geometries of these oligomers and their calculated HOMO and LUMO frontier orbitals are shown in Fig. 2. For all molecules, the HOMO wave function is delocalized through the entire backbones, and the LUMO wave function is mainly localized on the isoindigo units. As a result, the electron density distributions of HOMO and LUMO frontier orbitals suggest that the effective ICT is observed and indicates that the isoindigo unit has a strong electron-withdrawing effect due to its two lactam rings, which are consistent with the strong low-energy absorption band observed in Fig. 1. While the optimized molecular geometries of these copolymers were further analyzed, the coplanarity of these copolymers can be estimated by calculating the dihedral angle between CPDT and isoindigo units. The dihedral angles of the copolymers are listed in column 5 from left of Table 2. PC8I8 has the lowest dihedral angle as 14°, indicating that the backbone of PC8I8 is highly coplanar. Whereas PCeIe shows the highest dihedral angle as 20°, suggesting that the branched side chains attached on both the donor unit and the acceptor unit cause more twisting than the other three copolymers. As we compared the dihedral angle of PC8Ie and PCeI8, which are 17° and 18° respectively, the results indicate that the branched side chain attached on the

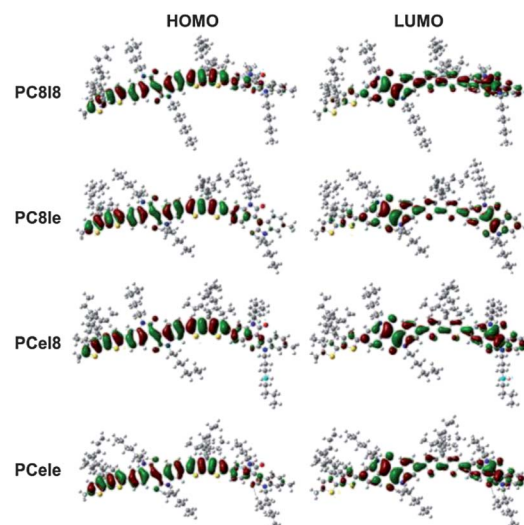


**Fig. 2** Calculated HOMO (left) and LUMO (right) frontier orbitals of PC8I8, PC8Ie, PCeI8 and PCeIe with two repeating units.

CPDT unit has a more steric hindrance effect on coplanarity of the backbone. These results are consistent with the optical properties discussed in the previous section and can be used as the motif in the design of other D–A type copolymers with various side chains.

### Electrochemical properties

The HOMO and LUMO energy levels of the copolymers are significant factors for determining the solar cell efficiency. The difference between LUMO of copolymers and LUMO of PCBM is able to influence the driving force for effective charge separation. The offset between HOMO of copolymers and LUMO of PCBM is related to the  $V_{oc}$  of corresponding PSCs.<sup>25</sup> Cyclic voltammetry is generally performed to calculate the HOMO and LUMO energy levels of conducting polymers. From the onset oxidation and reduction potentials determined in cyclic voltammograms, the corresponding HOMO and LUMO energy levels can be obtained respectively. Fig. 3 shows the cyclic voltammograms of copolymer films coated on ITO glass and recorded in TBAF/acetonitrile using Ag/Ag<sup>+</sup> as the reference electrode. All copolymers exhibit reversible oxidation/re-reduction processes in the positive potential region and reduction/re-oxidation processes in the negative potential region, indicating that these copolymers possess the unique ambipolar property. Interestingly, the current in the negative potential region is two times larger than that in the positive potential region. The reason for this phenomenon is not clear and is currently under investigation. The HOMO and LUMO energy levels of the copolymers were calculated according to the following equation<sup>38</sup> using ferrocene (Fc) as the internal standard,

$$E_{\text{HOMO}}(\text{e.V.}) = -(E_{\text{onset,ox.vs.Fc}^+/\text{Fc}} + 5.13)$$

$$E_{\text{LUMO}}(\text{e.V.}) = -(E_{\text{onset,red.vs.Fc}^+/\text{Fc}} + 5.13)$$

The results are summarized in columns 6, 7, 8, 9, and 10 from left of Table 2. The onset oxidation potentials of PC8I8, PC8Ie, PCeI8 and PCeIe are located at 0.11 V, 0.18 V, 0.20 V and

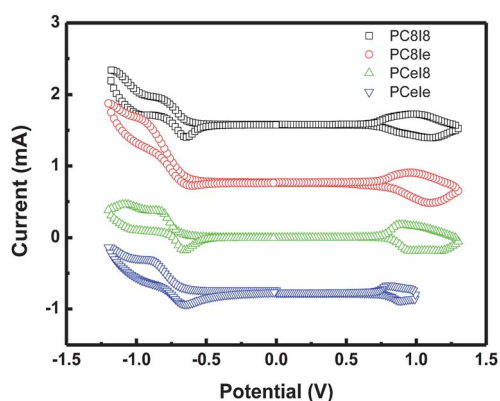


**Fig. 3** Cyclic voltammograms of different copolymer films coated on a ITO-coated glass in TBAF/acetonitrile solution. Open square: PC8I8; open circle: PC8Ie; open triangle: PCeI8; open inverted triangle: PCeIe.

0.32 V respectively, leading to the corresponding HOMO energy levels of the copolymers as  $-5.24$  eV,  $-5.31$  eV,  $-5.33$  eV and  $-5.45$  eV respectively. The results indicate that the HOMO energy level of the copolymers is decreased with decreasing coplanarity of the copolymers. The deep HOMO energy level of the copolymers suggests that all copolymers are air stable and have desired high open circuit voltage for solar cells.<sup>39</sup> On the other hand, the onset reduction potentials of PC8I8, PC8Ie, PCeI8 and PCeIe are positioned at  $-1.24$  eV,  $-1.25$  eV,  $-1.28$  eV and  $-1.17$  eV, respectively, resulting in the corresponding LUMO energy levels of the copolymers  $-3.89$  eV,  $-3.88$  eV,  $-3.85$  eV and  $-3.96$  eV respectively. No obvious trend related to the side chain effect can be observed. However, the LUMO energy levels of the copolymers are aligned with PCBM, thus good charge separation can be obtained. In summary, the nature of side chains has a large influence on the HOMO levels of polymers, whereas the effect on their LUMO levels is minor. The electrochemical band gaps of PC8I8, PC8Ie, PCeI8 and PCeIe are in the increasing order of 1.35 eV, 1.43 eV, 1.48 eV and 1.49 eV which show a similar trend as the optical band gap. Again, it demonstrates that by increasing the steric hindrance (branched side chains), the band gap is increased due to the lowered HOMO energy level and the reduction of effective ICT.

### Morphology of the blends of copolymer and PCBM

The active layer of polymer solar cells is made from the blend of copolymer and PCBM. For a high efficiency polymer solar cell, it is critical to manipulate the morphology of the blend to have the largest interfaces and longest continuous pathways for efficient charge separation and transport.<sup>40,41</sup> The morphologies of the different blend ratios from different side chain copolymers and with or without DIO were investigated by using AFM, as shown in Fig. 4 and Fig. S9–S12 in the ESI.† While the copolymers were blended with PCBM without DIO at either blend ratio of 1 : 1 or 1 : 2, phase separations are clearly observed for four copolymers. With the 1 : 1 blend ratio, the domain size of the PCBM rich phase (light color) for PC8I8, PC8Ie, PCeI8 is very similar (Fig. S9a, S10a, S11a†). The domain size of PCeIe (Fig. S12a†) is much larger than the other three copolymers which indicate that the miscibility of PCeIe with PCBM is the lowest among four copolymers. The increased solubility of PCeIe in chlorobenzene may cause the solubility of PCBM to be decreased and formed large extent of phase separation. The side chain effect is more pronounced for the blend ratio of 1 : 2 as shown in Fig. 4a–d due to the presence of excess PCBM. It is interesting to note that, with a blend ratio of 1 : 2, the phase separation of PCeIe has the largest domain size of the PCBM rich phase, whereas the PC8I8 has the smallest one. The results again confirm that the speculation of polymer solubility differences causes the formation of different domain sizes of each phase.

The shape of the side chain really plays the vital role for the domain size of phase separation in the blend. This investigation provides new insights into how the side chain structure can manipulate the domain size of phase separation which is the determining factor for the performance of the solar cell.

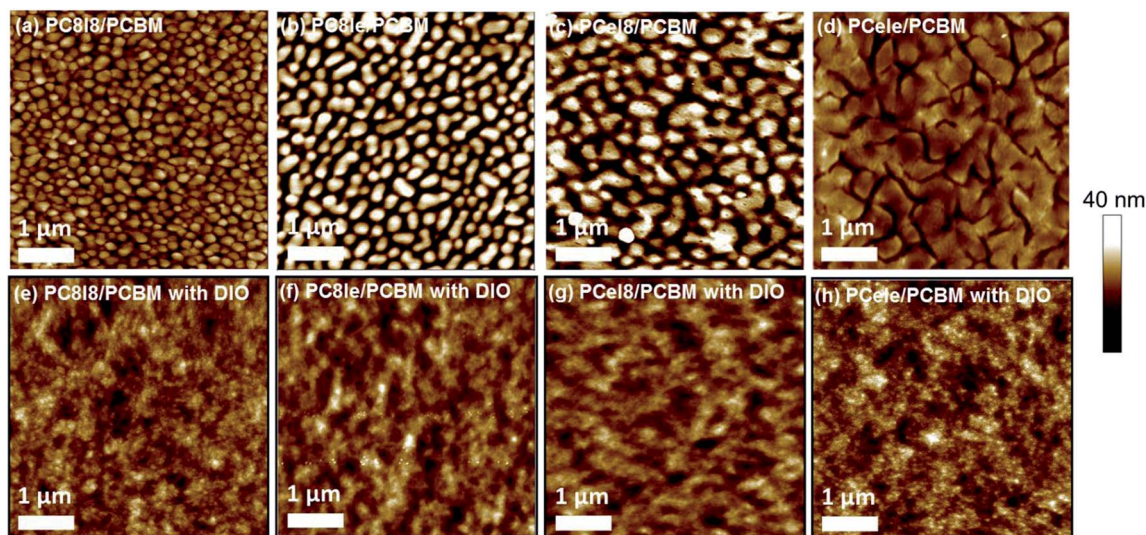


**Fig. 4** Surface morphology of different isoindigo polymer/PCBM (1 : 2) blend films using chlorobenzene as the solvent without DIO: (a) PC8I8, (b) PC8Ie, (c) PCeI8 and (d) PCeIe; with 3 vol% DIO: (e) PC8I8, (f) PC8Ie, (g) PCeI8 and (h) PCeIe.

The domain size without DIO of the PCBM rich phase (light color) is rather large and not in a long continuous path, which will result in a lower efficiency of the solar cell. It is known that the addition of DIO will increase the affinity of the low band gap D-A copolymer to PCBM to form the desired nanomorphology, where the phase separation becomes smaller and more continuous.<sup>42</sup> Thus, we added 3 vol% DIO as the processing additive in the blends using chlorobenzene as a solvent to prepare the thin film of the active layer. The resulting morphologies of thin films are shown in Fig. 4e–h for the 1 : 2 blends and Fig. S9c, S10c, S11c and S12c† for the 1 : 1 blends. The domain of the PCBM rich phase becomes continuous but the exact dimension cannot be resolved clearly. The domain size of the PCBM rich phase is again larger for the 1 : 2 blends due to the large extent of phase separation. It is worth noting that although the AFM measurements provide useful and preliminary morphological information, this technique could only probe the surface structures.<sup>43</sup> To thoroughly investigate the morphology inside the active layer, the detailed analysis of the domain size of DIO added blends using GISAXS and GIWAXS is currently under way and will be reported in the near future.

### Photovoltaic properties

In order to examine how the steric hindrance of side chains either attached on the donor unit or acceptor unit affects the device performance and the potential of these copolymers in solar cell applications, the bulk heterojunction PSCs were fabricated with the conventional device configuration of ITO/PEDOT:PSS/copolymer:PCBM(w/w)/Ca/Al. We have investigated the effect of different blend ratios of polymer and PCBM on the performance of solar cells using chlorobenzene as the solvent plus 3 vol% DIO for processing. The blend ratios are ranged from 1 : 0.5 to 1 : 3. In this work, the device has an active area of 4 mm<sup>2</sup> and was measured under simulated 100 mW cm<sup>-2</sup>, AM

1.5G illumination. The open-circuit voltage ( $V_{oc}$ ), short circuit current ( $J_{sc}$ ), fill factor (FF), and power conversion efficiency (PCE) of devices fabricated using different blend ratios of polymer and PCBM are tabulated in the ESI of Table S1.† The highest  $V_{oc}$  of 0.80 V is obtained for PCeIe, while the lowest  $V_{oc}$  of 0.66 V is observed for PC8I8. In general, the  $V_{oc}$  of these four copolymers has the increasing order of PC8I8 < PC8Ie < PCeI8 < PCeIe at all the blend ratios. The results show the same trend as the HOMO level of these copolymers discussed in the section of electrochemical properties. The lower is the HOMO level of the polymer the higher becomes the  $V_{oc}$ , because the  $V_{oc}$  is usually associated with the energy difference between the LUMO level of the acceptor (A) and the HOMO level of the donor (D). It is interesting to note that PC8I8 and PCeI8 have higher  $J_{sc}$  at the blend of 1 : 2 while PC8Ie and PCeIe have higher  $J_{sc}$  at the blend of 1 : 1. The results may be because the linear side chain on the isoindigo unit can accommodate more PCBM for efficient charge transport. As we carefully scrutinized these results, the side chains either linear or branched attached on the donor unit have less influence on the optimized blend ratio. However, when the linear side chain is attached on the acceptor unit, the amount of PCBM can be increased to facilitate the  $J_{sc}$ , thus achieving the high PCE, whereas the  $J_{sc}$  is deteriorated by adding an excessive amount of PCBM as the branched side chain is attached on the acceptor unit. The branched side chain on the acceptor unit of the copolymer always results in low FF for devices fabricated from the blend ratio higher than 1 : 1. The results may be due to the ease of phase separation and higher charge recombination for copolymers containing branched side chains. The fill factor of all the devices is less than 50% except PC8I8 at the blend ratio of 1 : 2.

Fig. 5 shows the typical current density *versus* voltage ( $J$ - $V$ ) curve of the devices fabricated by the optimized blend ratio of copolymer and PCBM. The results are summarized in Table 3. The PCeIe:PCBM device has the highest cell efficiency of 4.0%

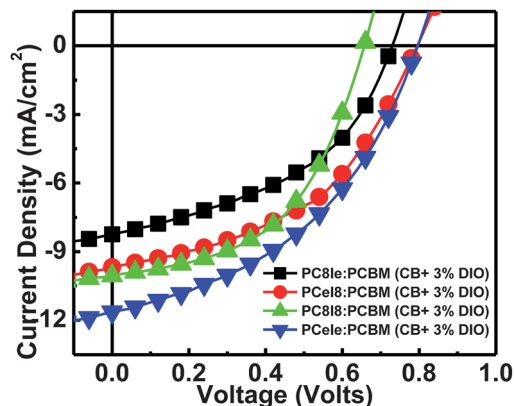


**Fig. 5**  $J$ - $V$  curves of solar cells fabricated from the optimized blend ratio of different copolymers with PC61BM using chlorobenzene plus 3 vol% DIO as the solvent. PC8I8/PCBM (1 : 2, black square), PC8Ie/PCBM (1 : 1, red circle), PCeI8/PCBM (1 : 1, green triangle), PCeIe/PCBM (1 : 1.5, blue inverted triangle).

**Table 3** Summary of device performances of optimized blended ratio of copolymers/PC<sub>61</sub>BM containing 3% DIO as the processing additive

Active layer	Ratio	$V_{oc}$ (V)	$J_{sc}$ (mA cm <sup>-2</sup> )	FF (%)	PCE <sup>a</sup> (%)
PC8I8:PCBM	1 : 2	0.66	10.1	50.2	2.6 ± 0.3 (3.3)
PC8Ie:PCBM	1 : 1	0.73	8.2	44.5	2.2 ± 0.3 (2.7)
PCeI8:PCBM	1 : 2	0.79	9.7	46.9	3.0 ± 0.3 (3.6)
PCeIe:PCBM	1 : 1.5	0.80	11.6	43.0	3.5 ± 0.4 (4.0)

<sup>a</sup> The standard deviation of power conversion efficiency (PCE) of the devices for each blend is present with the highest PCE in parentheses.

whereas the PC8Ie:PCBM device exhibits the lowest efficiency of 2.7%. The external quantum efficiency (EQE) profiles of the devices are shown in Fig. 6. The calculated  $J_{sc}$  from the EQE profiles is close to the  $J_{sc}$  from  $J$ - $V$  curves and demonstrate no lost current from other pathways. The solar cell performance of these isoindigo based copolymer is expected to be further improved by (1) using other kinds of processing solvents and additives to achieve the most desirable size of nanodomain

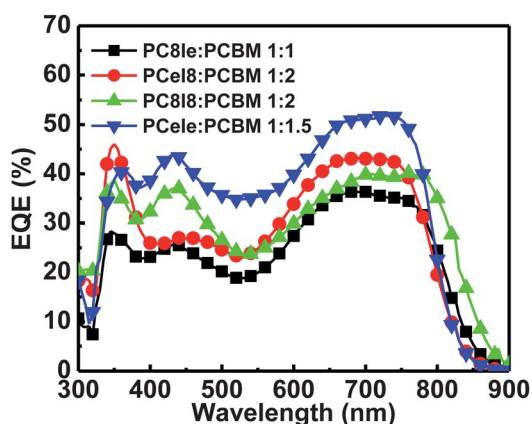


**Fig. 6** EQE profiles of solar cells fabricated from the optimized blend ratio of different copolymers with PCBM.

phase separation and to reduce charge recombination and (2) modifying the interfaces between the active layer and charge transport layer to extract the charge more efficiently toward the electrode. Both approaches are currently under investigations and the results will be reported in the near future.

## Conclusion

We have synthesized a series of soluble D-A polymers with CPDT and isoindigo *via* the Stille cross-coupling reaction. Using these synthetic methods, the materials from monomers to polymers can be produced in large quantity with the potential to scale up. Two kinds of side chains, octyl (linear) and 2-ethylhexyl (branched), were decorated on a donor unit and acceptor unit, resulting in four copolymers denoted as PC8I8, PC8Ie, PCeI8 and PCeIe. From optical property results, these copolymers have broad absorption from the ICT effect. The steric hindrance effects of side chains on the copolymers cause the reduction of ICT and thus increase their optical band gaps. Theoretical calculation also supports the ICT effect of these copolymers from the electron density distribution of HOMO and LUMO frontier orbitals and the reduction of ICT by analyzing the dihedral angle between the CPDT unit and isoindigo unit. From electrochemical property results, it can be concluded that the copolymers have deep HOMO energy levels and the HOMO energy levels can be lowered by increasing the steric hindrance, whereas the steric hindrance has less influence on the LUMO energy level. From photovoltaic property results, the linear side chain can accommodate more PCBM for higher  $J_{sc}$  whereas the branched side chain assists the phase separation for effective charge separation. The type of side chain attached on the acceptor unit is a dominant factor to determine the solar cell performance. Finally, the highest PCE of 4.0% was obtained from a copolymer containing two branched side chains on the acceptor unit (PCeIe). The results of this study provide new insights into how the structure of the side chain affects the morphology, optoelectronic and photovoltaic properties of the alternating donor-acceptor copolymer for bulk heterojunction solar cell applications.

## Acknowledgements

We gratefully acknowledge the financial support from the National Science Council of Taiwan (NSC 99-2221-E-002-020-MY3, 101-2120-M-002-003, 101-3113-E-002-010, 102-3113-P-002-027). We also thank the Department of Chemistry of National Taiwan University for the use of their NMR spectrometer. We thank the National Center of High-Performance Computing for the use of their ALPS Cluster.

## Notes and references

- 1 J. W. Chen and Y. Cao, *Acc. Chem. Res.*, 2009, **42**, 1709–1718.
- 2 G. Dennler, M. C. Scharber and C. J. Brabec, *Adv. Mater.*, 2009, **21**, 1323–1338.
- 3 C. Li, M. Y. Liu, N. G. Pschirer, M. Baumgarten and K. Mullen, *Chem. Rev.*, 2010, **110**, 6817–6855.

- 4 T. D. Nielsen, C. Cruickshank, S. Foged, J. Thorsen and F. C. Krebs, *Sol. Energy Mater. Sol. Cells*, 2010, **94**, 1553–1571.
- 5 C. J. Brabec, S. Gowrisanker, J. J. M. Halls, D. Laird, S. J. Jia and S. P. Williams, *Adv. Mater.*, 2010, **22**, 3839–3856.
- 6 H. Zhou, L. Yang and W. You, *Macromolecules*, 2012, **45**, 607–632.
- 7 P. L. T. Boudreault, A. Najari and M. Leclerc, *Chem. Mater.*, 2011, **23**, 456–469.
- 8 M. Jarosz, M. Puchalska, K. Polec-Pawlak, I. Zadrozna and H. Hryszko, *J. Mass Spectrom.*, 2004, **39**, 1441–1449.
- 9 J. G. Mei, K. R. Graham, R. Stalder and J. R. Reynolds, *Org. Lett.*, 2010, **12**, 660–663.
- 10 R. Stalder, J. Mei and J. R. Reynolds, *Macromolecules*, 2010, **43**, 8348–8352.
- 11 Z. Ma, E. Wang, M. E. Jarvid, P. Henriksson, O. Inganas, F. Zhang and M. R. Andersson, *J. Mater. Chem.*, 2012, **22**, 2306–2314.
- 12 Z. F. Ma, E. G. Wang, K. Vandewal, M. R. Andersson and F. L. Zhang, *Appl. Phys. Lett.*, 2011, **99**, 143302–143304.
- 13 R. Stalder, C. Grand, J. Subbiah, F. So and J. R. Reynolds, *Polym. Chem.*, 2012, **3**, 89–92.
- 14 E. Wang, Z. Ma, Z. Zhang, K. Vandewal, P. Henriksson, O. Inganäs, F. Zhang and M. R. Andersson, *J. Am. Chem. Soc.*, 2011, **133**, 14244–14247.
- 15 E. G. Wang, Z. F. Ma, Z. Zhang, P. Henriksson, O. Inganas, F. L. Zhang and M. R. Andersson, *Chem. Commun.*, 2011, **47**, 4908–4910.
- 16 G. Zhang, Y. Fu, Z. Xie and Q. Zhang, *Macromolecules*, 2011, **44**, 1414–1420.
- 17 Y. P. Zou, B. Liu, B. Peng, B. Zhao, K. L. Huang, Y. H. He and C. Y. Pan, *Polym. Chem.*, 2011, **2**, 1156–1162.
- 18 T. Lei, Y. Cao, Y. Fan, C.-J. Liu, S.-C. Yuan and J. Pei, *J. Am. Chem. Soc.*, 2011, **133**, 6099–6101.
- 19 Z. Li, Y. Zhang, S.-W. Tsang, X. Du, J. Zhou, Y. Tao and J. Ding, *J. Phys. Chem. C*, 2011, **115**, 18002–18009.
- 20 L. Biniek, S. Fall, C. L. Chochos, D. V. Anokhin, D. A. Ivanov, N. Leclerc, P. Lévêque and T. Heiser, *Macromolecules*, 2010, **43**, 9779–9786.
- 21 H. X. Zhou, L. Q. Yang, S. Q. Xiao, S. B. Liu and W. You, *Macromolecules*, 2010, **43**, 811–820.
- 22 S. Massip, P. M. Oberhumer, G. Tu, S. Albert-Seifried, W. T. S. Huck, R. H. Friend and N. C. Greenham, *J. Phys. Chem. C*, 2011, **115**, 25046–25055.
- 23 L. Q. Yang, H. X. Zhou and W. You, *J. Phys. Chem. C*, 2010, **114**, 16793–16800.
- 24 H. X. Zhou, L. Q. Yang, S. Stoneking and W. You, *ACS Appl. Mater. Interfaces*, 2010, **2**, 1377–1383.
- 25 M. C. Scharber, D. Muehler, M. Koppe, P. Denk, C. Waldauf, A. J. Heeger and C. L. Brabec, *Adv. Mater.*, 2006, **18**, 789–794.
- 26 J. H. Park and B. Y. Lee, *Bull. Korean Chem. Soc.*, 2010, **31**, 1064–1066.
- 27 A. T. Jeffries, K. C. Moore, D. M. Ondeyka, A. W. Springsteen and D. W. H. Macdowell, *J. Org. Chem.*, 1981, **46**, 2885–2889.
- 28 P. Coppo, D. C. Cupertino, S. G. Yeates and M. L. Turner, *Macromolecules*, 2003, **36**, 2705–2711.
- 29 P. Jordens, G. Rawson and H. Wynberg, *J. Chem. Soc. C*, 1970, 273–277.
- 30 J. Z. Brzezinski and J. R. Reynolds, *Synthesis*, 2002, 1053–1056.
- 31 S. Barlow, S. A. Odom, K. Lancaster, Y. A. Getmanenko, R. Mason, V. Coropceanu, J. L. Bredas and S. R. Marder, *J. Phys. Chem. B*, 2010, **114**, 14397–14407.
- 32 G. W. T. M. J. Frisch, H. B. Schlegel, G. E. Scuseria, M. A. Robb, J. R. Cheeseman, G. Scalmani, V. Barone, B. Mennucci, G. A. Petersson, H. Nakatsuji, M. Caricato, X. Li, H. P. Hratchian, A. F. Izmaylov, J. Bloino, G. Zheng, J. L. Sonnenberg, M. Hada, M. Ehara, K. Toyota, R. Fukuda, J. Hasegawa, M. Ishida, T. Nakajima, Y. Honda, O. Kitao, H. Nakai, T. Vreven, J. A. Montgomery Jr, J. E. Peralta, F. Ogliaro, M. Bearpark, J. J. Heyd, E. Brothers, K. N. Kudin, V. N. Staroverov, R. Kobayashi, J. Normand, K. Raghavachari, A. Rendell, J. C. Burant, S. S. Iyengar, J. Tomasi, M. Cossi, N. Rega, J. M. Millam, M. Klene, J. E. Knox, J. B. Cross, V. Bakken, C. Adamo, J. Jaramillo, R. Gomperts, R. E. Stratmann, O. Yazyev, A. J. Austin, R. Cammi, C. Pomelli, J. W. Ochterski, R. L. Martin, K. Morokuma, V. G. Zakrzewski, G. A. Voth, P. Salvador, J. J. Dannenberg, S. Dapprich, A. D. Daniels, Ö. Farkas, J. B. Foresman, J. V. Ortiz, J. Cioslowski, and D. J. Fox, in *Gaussian 09, Revision A.1*, Gaussian, Inc., Wallingford CT, 2009.
- 33 A. D. Becke, *J. Chem. Phys.*, 1993, **98**, 5648–5652.
- 34 C. T. Lee, W. T. Yang and R. G. Parr, *Phys. Rev. B: Condens. Matter*, 1988, **37**, 785–789.
- 35 W. J. Hehre, R. Ditchfie and J. A. Pople, *J. Chem. Phys.*, 1972, **56**, 2257.
- 36 S. B. Darling, *J. Phys. Chem. B*, 2008, **112**, 8891–8895.
- 37 S. B. Darling and M. Sternberg, *J. Phys. Chem. B*, 2009, **113**, 6215–6218.
- 38 C. M. Cardona, W. Li, A. E. Kaifer, D. Stockdale and G. C. Bazan, *Adv. Mater.*, 2011, **23**, 2367–2371.
- 39 N. Blouin, A. Michaud, D. Gendron, S. Wakim, E. Blair, R. Neagu-Plesu, M. Belletete, G. Durocher, Y. Tao and M. Leclerc, *J. Am. Chem. Soc.*, 2008, **130**, 732–742.
- 40 M. Y. Chiu, U. S. Jeng, C. H. Su, K. S. Liang and K. H. Wei, *Adv. Mater.*, 2008, **20**, 2573–2578.
- 41 M. S. Su, C. Y. Kuo, M. C. Yuan, U. S. Jeng, C. J. Su and K. H. Wei, *Adv. Mater.*, 2011, **23**, 3315–3319.
- 42 S.-Y. Chang, H.-C. Liao, Y.-T. Shao, Y.-M. Sung, S.-H. Hsu, C.-C. Ho, W.-F. Su and Y.-F. Chen, *J. Mater. Chem. A*, 2013, **1**, 2447–2452.
- 43 W. Chen, M. P. Nikiforov and S. B. Darling, *Energy Environ. Sci.*, 2012, **5**, 8045–8074.